Drawdown of Atmospheric pCO_2 via Dynamic Particle Export Stoichiometry in the Ocean Twilight Zone

Tatsuro Tanioka[1,+,*], Katsumi Matsumoto[1], and Michael W. Lomas[2]

[1] Department of Earth & Environmental Sciences, University of Minnesota, Minneapolis, MN, USA
[2] Bigelow Laboratory for Ocean Sciences, East Boothbay, ME, USA

**Correspondence to*: Tatsuro Tanioka (tatsurt@uci.edu)

[+] Current affiliation: Department of Earth System Science, University of California Irvine, Irvine, CA, USA

Key Points:

- New global data compilation of particle flux shows systematic increase in carbon (C) to phosphorus (P) export stoichiometry with depth.
- Increase in the C:P flux ratio in the twilight zone can lead to a significant drawdown of atmospheric pCO_2.
- Further studies to elucidating mechanisms leading to spatiotemporal C:P flux variability in the twilight zone are required.

Abstract

The strength of the biological soft tissue pump in the ocean critically depends on how much organic carbon is produced via photosynthesis and how efficiently the carbon is transferred to the ocean interior. For a given amount of limiting nutrient, phosphate, soft tissue pump would be strengthened if the carbon (C) to phosphorus (P) ratio of sinking organic matter increases as the remineralization length scale of C increases. Here, we present a new data compilation of particle flux stoichiometry and show that C:P of sinking particulate organic matter (POM) in the ocean twilight zone is systematically higher than the Redfield C:P and the C:P ratio of surface suspended POM. We further demonstrate using a physics-biology coupled global ocean model combined with a theory from first principles that an increase in C:P flux ratio in the ocean's twilight zone can lead to considerable variability in atmospheric pCO_2.

Plain Language Summary

The ocean's twilight zone, located below the ocean's sunlit zone, is a region where many critical biogeochemical processes occur. Most notably, organic matter produced by primary producers in the surface ocean is consumed by microbes and animals here. How efficiently these organic matters are degraded exerts essential controls on atmospheric carbon dioxide levels and energy transfer in the marine food web. Here we show using new global data that organic carbon and phosphorus particles are degraded at different rates. This leads to a considerable change in carbon to phosphorus ratio at depth. We incorporate this variability into the 3D ocean model to show that such change can significantly perturb the global carbon cycle. The study ultimately highlights the need to accurately characterize the ocean's role in climate change by studying the particle dynamics in the twilight zone.

1. Introduction

Understanding the processes that transfer, transform, and store carbon in the ocean interior is critical for gaining a better picture of the evolution of the climate system (Sigman & Boyle, 2000). The biological carbon pump is one of the critical mechanisms whereby marine phytoplankton convert inorganic carbon into organic carbon via photosynthesis, and that carbon is subsequently transported into the ocean interior. The majority of sinking particulate organic matter (POM) is progressively consumed and respired by heterotrophic organisms and fuels their growth in the twilight zone (200 – 1000 m) of the ocean (Buesseler et al., 2007; Giering et al., 2014). If POM can penetrate deeper into the water column without being degraded in the twilight zone, more carbon can be

sequestered in the ocean as the residence time of the deep ocean is much longer than that of the surface ocean (Kwon et al., 2009; Matsumoto, 2007).

The conventional thinking is that oceanic carbon storage due to the biological carbon pump is proportional to the total inventory of phosphate in the interior ocean that arrived through the biological "regenerated" pathway (Ito & Follows, 2005; Marinov, Gnanadesikan, et al., 2008). This hypothesis assumes a fixed C:P stoichiometry, where carbon transfer efficiency into the ocean interior is tightly coupled to the transfer of phosphate from surface to depth. Under this framework, an increase in POM transfer efficiency and associated drawdown on atmospheric pCO_2 will rapidly deplete surface nutrients, most notably in the North Atlantic and the Southern Ocean regions, where most deep water is formed (Sarmiento & Toggweiler, 1984).

Another school of thought proposes that the biological carbon pump can be strengthened if the C:P ratio of sinking POM increases with depth (Broecker, 1982a, 1982b; Knauer et al., 1979; Menzel & Ryther, 1964). This strengthening can happen if the remineralization length scale of POC becomes longer than that of POP such that C:P of the sinking POM exceeds C:P of upward inorganic flux (Christian et al., 1997). The seminal study by Menzel and Ryther (1964) demonstrated by sampling POM in the mesopelagic region of Western North Atlantic that particulate phosphorus is remineralized more quickly than particulate carbon or nitrogen. Subsequent studies based on sediment traps and hydrographic studies have supported this theory (Knauer et al., 1979; J. H. Martin et al., 1987; Minster & Boulahdid, 1987). Furthermore, a recent inverse model study (Teng et al., 2014) argues that depth-dependent change in C:P of sinking POM can better explain observed inorganic carbon and phosphate distribution than the model with fixed a C:P.

Here, we provide new lines of evidence for linking vertical variability in the C:P ratio of sinking POM in the twilight zone to carbon storage by using a compilation of recently published data and the time-series data from the Bermuda Atlantic Time-series Study (BATS). We then use a global ocean biogeochemistry model, combined with a theory derived from first principles, to illustrate that increase in the twilight zone C:P ratio could significantly strengthen ocean biological carbon pump and drawdown of atmospheric CO_2. Previous modeling studies explored the effect of changes in C:P in the surface POM involving phytoplankton on carbon export (Galbraith & Martiny, 2015; Kwiatkowski et al., 2018; Moreno et al., 2018; Ödalen et al., 2020; Tanioka & Matsumoto, 2017) but not the subsurface processes that change C:P. Our 3D modeling study investigates the

effects of C:P changes both at the surface and in the subsurface ocean that also involve stoichiometric interaction between phytoplankton and zooplankton.

2. Methods

2.1 Data compilation of sinking POM

We compiled a new set of data on POC and POP fluxes based on previous compilations by Antia (2005), Faul et al. (2005), and Paytan et al. (2003) to gather POC and POP sedimentary flux data that have been collected simultaneously. Total P is the sum of reactive P and detrital P, where reactive P is the sum of authigenic P and acid-insoluble organic P (Faul et al., 2005). We have excluded coastal samples, and samples from the Southern Ocean as these sites are influenced mainly by resuspended or advected P (Faul et al., 2005). Despite a wide range in sample treatment protocols, consistent trends across data indicate that the trends are not artifacts of sample processing or storage after collection (Faul et al., 2005).

We also included in our new data compilation several studies that were not included in the previous compilations (Benitez-Nelson et al., 2007; Engel et al., 2017; Grabowski et al., 2019; Karl et al., 2012; Lamborg et al., 2008; Lomas et al., 2010). As a quality control, we only include studies published after 2005 that report latitude and longitude information, and we took the average over the non-overlapping periods if multiple samples are taken from the same latitude and longitude. In addition, we limit our study to the samples below the epipelagic zone, operationally defined here as 100 m. Finally, for stations ALOHA and BATS, where multiple studies report sedimentary flux values, we selected the study by Grabowski et al. (2019) and Lomas et al. (2010) to represent the mean values for ALOHA and BATS, respectively. Selection processes based on the above criteria led to a total of 54 POC:POP flux ratio measurements (Table S1). We delineated each sample into separate oceanographic

107 regions (boundaries shown in Figure 1a) based on the 0.3 mmol m^{-3} contour of the annually averaged PO_4
108 concentration from World Ocean Atlas 2018 (Garcia et al., 2018).
109

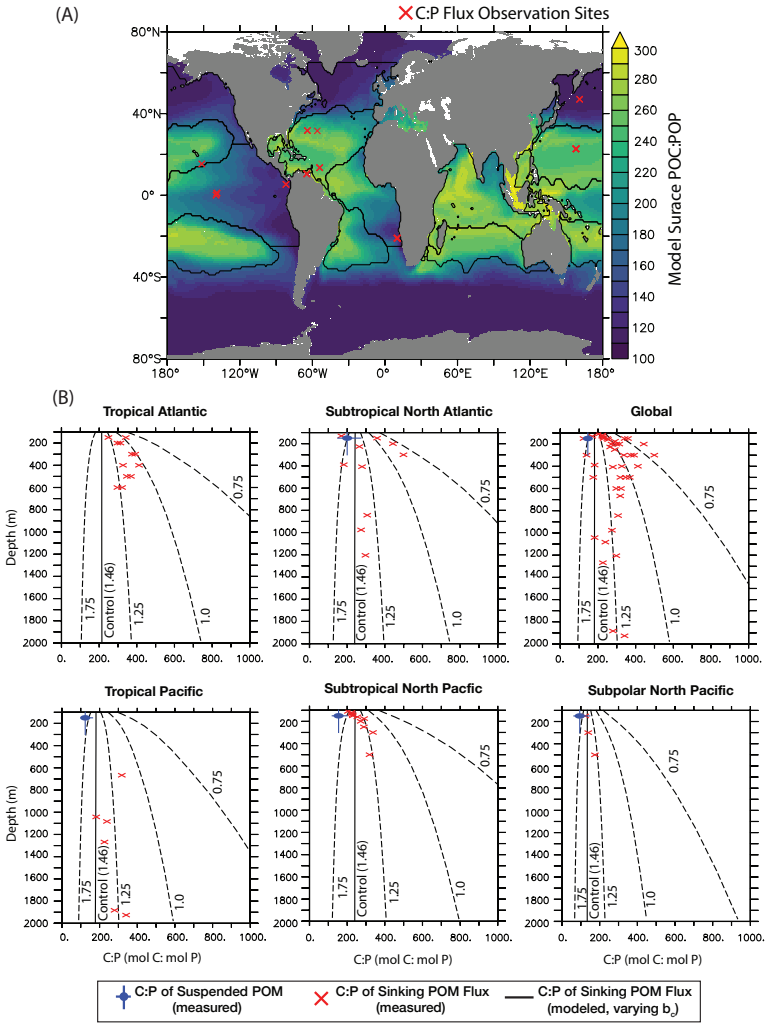

Figure 1. Depth profiles of C:P of sinking POM from our new data compilation. (a) Locations of samples collected shown with red crosses superimposed on the modeled C:P of suspended POM at the surface. The boundaries are based on the 0.3 mmol m^{-3} of the annually averaged surface PO_4 concentration. (b) Depth profile of C:P flux ratio of sinking POM (red cross) with C:P of suspended POM in the top 300 m (blue circle; Martiny et al., 2013). C:P flux ratios from a 3D model with different values of b_C (Martin *b* of POC) are shown with black dotted lines. Only the values between 100 and 2000 m are shown here.

In addition to the "snapshot" of particle flux measurements, we used the continuous sedimentary flux timeseries measurements of POC and POP fluxes from BATS (31° 40' N 064°10'W), collected from 2006 to 2019 at three different depths (150, 200, and 300 m). Using this data, we computed Martin b exponent ($F(z) \propto (z/z_0)^{-b}$) for POP and POC separately for each time point using 150 m as a reference depth z_0. POC and POP sedimentary particle flux from the BATS station were measured using the standard method previously described (Lomas et al., 2010) and are publicly available (http://bats.bios.edu; last access April 23, 2021). All statistical analyses were conducted in R version 4.0.4 (R Core Team, 2021).

2.2 Ocean Biogeochemical Model

2.2.1 General Overview

We conducted all numerical simulations by applying the transport matrix model (TMM) (Khatiwala, 2007; Khatiwala et al., 2005) as an efficient offline method to simulate the 3D transport of tracers in the global ocean. The Transport Matrices (TMs) used in this study are derived from the circulation of the Estimating the Circulation and Climate of the Ocean (ECCO) project, with a horizontal resolution of 1° by 1° and 23 levels in the vertical (Stammer et al., 2004). ECCO circulation field is optimized to best fit hydrographic and remote sensing observations as well as the mean age of water parcels constrained by transient tracers (radiocarbon and chlorofluorocarbons, CFCs) (Khatiwala et al., 2012).

TMM circulation field is coupled to Model of Oceanic Pelagic Stoichiometry (MOPS), a simple NPZD model with nine default prognostic variables: phosphate, nitrate, dissolved inorganic carbon, alkalinity, oxygen, dissolved organic phosphorus, detritus, a single class of phytoplankton, and a single class of zooplankton (Kriest & Oschlies, 2015). In the original MOPS, the central currency of the model is phosphorus and assumes a fixed stoichiometric ratio of C:N:P:-O_2 = 117:16:1:151. Phytoplankton growth is limited by light and nutrients (phosphate and nitrate), assuming that the most limiting resource determines the growth rate. Phytoplankton is grazed by zooplankton as described a Holling Type III function with a quadratic dependence on phytoplankton biomass. The model assumes that a fixed fraction (15%) of egestion, zooplankton mortality, and phytoplankton loss is released as DOP, and the rest becomes detritus. Attenuation of detritus (POP) down the water column is described via the Martin Curve: $F(z) \propto (z/z_0)^{-b}$, and we refer to parameter b as the "Martin b" throughout this paper. A fraction of detritus that reaches the seafloor is buried instantaneously, and the non-buried fraction is resuspended back into the water column. The global river runoff equivalent to the annual flux of total organic P buried in the previous year is resupplied to the surface box to close the phosphorus budget (Kriest & Oschlies,

2013). The key biogeochemical parameters, including the Martin *b* for POP, were objectively calibrated specifically for the ECCO transport matrix field to match observed PO_4, O_2, and NO_3 (Kriest et al., 2020; Figure S1).

2.2.2 Flexible C:P dynamics

This study added four new state variables related to organic carbon: phytoplankton carbon, zooplankton carbon, DOC, and detritus carbon (which we refer to as POC) to simulate the variable C:P ratio of organic matter. Phytoplankton P:C ratio in production layers is modeled using the power-law formulation as a function of ambient temperature and PO_4 (Tanioka & Matsumoto, 2017, 2020):

$$[P:C]_{PHY} = [P:C]_{PHY,ref} \cdot \left(\frac{[PO_4]}{[PO_4]_0}\right)^{s_{PO_4}^{P:C}} \cdot \left(\frac{T}{T_0}\right)^{s_T^{P:C}} \quad (1)$$

The exponents are the sensitivity factors determined by a meta-analysis (Tanioka and Matsumoto, 2020a), and the subscript "0" indicates the reference environmental values, where at these values, P:C equals the reference P:C (i.e., $[P:C]_{PHY,ref}$ = Redfield Ratio = 1:117). The complete list of parameters used in the model is provided in Table S4.

Zooplankton P:C ratio is flexible and computed as a function phytoplankton P:C in a power-law formulation:

$$[P:C]_{zoo} = [P:C]_{zoo,ref}{}^{1-H}[P:C]_{PHY}{}^{H} \quad (2)$$

where *H* is the homeostasis parameter, which takes a value of 0 when zooplankton P:C is completely homeostatic and a value of 1 when $[P:C]_{zoo}$ is directly proportional to $[P:C]_{PHY}$. In our study, we use *H* of 0.08 based on the meta-analysis by Persson et al. (2010) and assign the reference P:C of zooplankton, $[P:C]_{zoo,ref}$, equal to the Redfield ratio of 1:117. For zooplankton to maintain homeostatic C:P, zooplankton egests excess C into the environment as a new POC to cancel the mismatch between C:P of prey and the optimal C:P. Although studies suggest that 10-30% of POC ingested by zooplankton is released as DOC (Steinberg & Landry, 2017), we assume here for simplicity that all of the egested carbon goes to the POC pool.

For this study, we further assume that phytoplankton are always more C-rich than zooplankton (i.e., $[P:C]_{PHY} < [P:C]_{zoo}$) by setting hard-bound maximum $[P:C]_{PHY}$ to equal 1:117. With this simplification, zooplankton will only release excess C but not excess P. This ensures that the stoichiometry regulation of zooplankton will not affect values of inorganic nutrients and allows a fair comparison of model results across different sensitivity runs mentioned later. Some laboratory studies support our assumption that phytoplankton are more carbon-rich than zooplankton even under P-sufficient conditions (e.g., Boersma et al., 2009), and we believe that release of excess P by zooplankton occurs much less frequently than the release of excess C in most of the open ocean. However, future studies would be needed to accurately model C:P of both phytoplankton and zooplankton under P-sufficient conditions and how the release of excess P via stoichiometric regulation could impact biogeochemical fluxes.

Kinetic parameters such as rate constants (λ) for remineralization for various source-minus-sink terms of POC and DOC are identical to those of POP and DOP, respectively. In the control run, the same Martin parameter (b = 1.46) is assigned to both POC and POP so that there is no preferential remineralization of one over the other. This Marin b value of 1.46 is specifically derived for MOPS (Kriest et al., 2020) and is different from the original Martin b parameter of 0.86 (J. H. Martin et al., 1987). A full description of source-minus-sink terms of the ocean biogeochemistry model is given in Text S1.

2.2.3 Numerical experimental setup

We initialized MOPS for 3000 years under the constant climate scenario with fixed atmospheric pCO_2 at 280 ppm using monthly mean TMs, wind speed, temperature, salinity, and spatially variable P:C uptake ratios for phytoplankton and zooplankton following Equations (1) and (2). Our modeled surface POC:POP (Figure 1a) generally follows the observed latitudinal pattern with high values in the nutrient-deplete warm subtropical gyres and lowest values in the nutrient-rich subpolar and polar regions (Figure S2). Following the 3000-year spin-up run, at which point the model has reached a steady state, we conducted sensitivity experiments to evaluate the response of the soft tissue pump to change in the C:P ratio of sinking POM. We systematically varied the Martin b parameter for POC (b_C) between 0.5 and 1.75 while keeping the Martin parameter for POP (b_P) constant at 1.46 to allow preferential remineralization of POP and POC over one another. When b_C is less than the fixed b_P of 1.46, POP is preferentially remineralized over POC, and vice versa when b_C is greater than 1.46. Keeping the POP attenuation profile constant and not considering CO_2 radiative feedback across sensitivity runs ensures that the concentrations of all non-carbon tracers are identical in each sensitivity run. This way, we can effectively isolate the effect of C:P on the strength of soft-tissue carbon pump without changing preformed and regenerate phosphate

concentrations. We conducted each sensitivity run for 1000 years following a 3000-year control run to a new equilibrium state. The total amount of carbon in the ocean-atmosphere system remains constant as C:P of river supply, and burial are fixed at 117, and phosphate inventory is steady. We assumed OCMIP-type, fast gas exchange protocol where surface ocean pCO_2 at each time step is in equilibrium with atmospheric pCO_2. In addition, alkalinity is kept spatially uniform in all the sensitivity runs. These assumptions used in previous studies (Marinov, Follows, et al., 2008; Marinov, Gnanadesikan, et al., 2008) are essential for isolating the effects of the soft-tissue pump on atmospheric pCO_2 and comparing model results with the theoretical predictions.

3. Results

3.1 Depth-dependent change in POC:POP flux ratio

Our new data compilation indicates that the C:P ratio of sinking POM in the twilight zone is generally higher than the regionally averaged C:P of suspended POM in the top 300 m in the overlying water column (Figure 1b). Observed C:P flux ratios in the twilight zone range between 83:1 and 500:1 with the global median of 280:1 (Table S2). This is approximately a factor of two greater than the global weighted mean C:P of suspended matter of 146:1 in the top 50 m (Martiny et al., 2013). Regionally, the tropical Atlantic region exhibits the highest C:P flux ratio of 334:1 in the twilight zone, followed by tropical Pacific (C:P = 274:1) and the Subtropical North Atlantic (C:P = 274:1). The Subpolar North Pacific region shows the lowest C:P flux ratio of 142:1 but is still higher than the mean surface suspended particle C:P of 94:1 in that region (Martiny et al., 2013, 2014). Although the limited sample size and averaging across multiple depth horizons preclude us from making firm conclusions, our new data compilation confirms previous findings that the mean C:P flux ratio of sinking organic matter in the mesopelagic zone is generally higher than the C:P of suspended POM (Knauer et al., 1979; Menzel & Ryther, 1964).

In addition to the global compilation, POM dynamics in the BATS ocean time-series provide continuous sedimentary POC and POP fluxes in the top mesopelagic depths (150 ~ 300 m) from 2003 to 2019. Median Martin *b* is significantly higher for POP (b_P = 1.28*)* compared to POC (b_C = 0.98), which indicate a shallower remineralization profile of POP over POC (Figure 2b, Table S3). There were no temporal shifts in the magnitude of Martin *b* for POP and POC between 2006 and 2019, but the systematic difference in Martin *b* for POP and POC at BATS is persistent over time (Figure 2a), indicating that preferential remineralization of POP over POC is a prevalent feature in the subtropical region.

3.2 Effects of variable C:P export stoichiometry on pCO_2: Theory and Model Results

Following the first-principle argument (Ito & Follows, 2005; Marinov, Follows, et al., 2008; Marinov, Gnanadesikan, et al., 2008), the total ocean carbon storage due to soft-tissue pump (OCS_{soft}) can be determined by the remineralized PO_4 inventory ($\overline{PO_{4remin}}$) scaled by a global mean C:P ratio of remineralization ($r_{C:P}$):

$$OCS_{soft} = r_{C:P} \cdot \overline{PO_{4remin}} \cdot V_{oc}$$
$$= r_{C:P} \cdot (\overline{PO_4} - \overline{PO_{4pref}}) \cdot V_{oc} \quad (3)$$

where V_{OC} is the ocean volume, and $\overline{PO_4}$ (= 2.14 mmol m^{-3}) and $\overline{PO_{4pref}}$ (= 1.09 mmol m^{-3}) are global volume averages for total PO_4 and preformed PO_4, respectively obtained from our MOPS-ECCO model simulation at steady state. Preformed PO_4 in the ocean interior in model simulations is computed from AOU and fixed $-O_2$:P of 151.1. Our modeled mean PO_4 compares well with observed global mean PO_4 of 2.26 mmol m^{-3}, and mean observed preformed PO_4 concentrations of 2.2 mmol m^{-3} and 0.8 mmol m^{-3} for Antarctic Bottom Water (AABW) and North Atlantic Deepwater (NADW), respectively (Duteil et al., 2012).

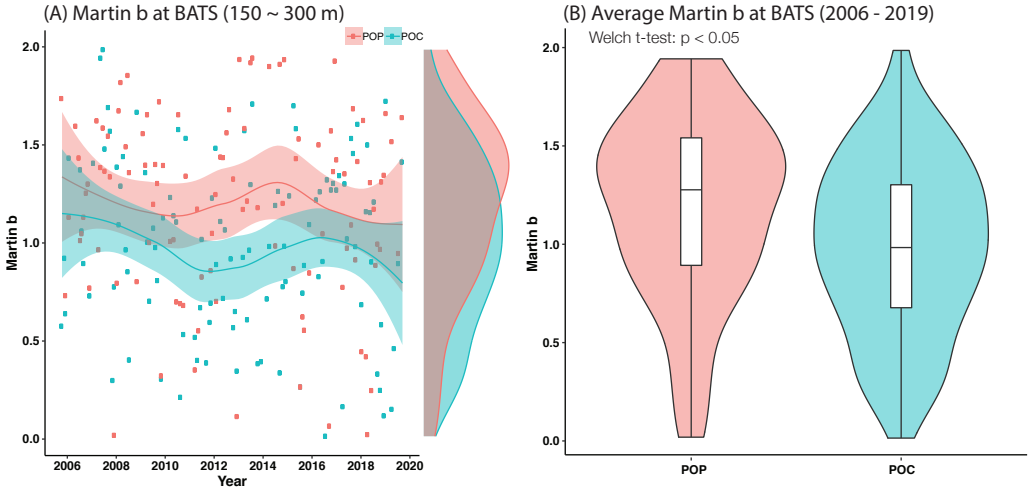

Figure 2. Martin *b* estimated from POC and POP flux profiles at BATS. (a) Time-series of the Martin *b* parameters from 2006 to 2019 for POP (red) and POC (blue). Smooth lines are Locally Weighted Least Squares Regression. (b) Violin plot for average Martin *b* values at BATS from 2006 to 2019. The whiskers of the box plot cover 95% confidence interval and the box shows 25%, 50%, and 75% percentiles. The median values of b_P *and* b_C are 1.28 and 0.98, respectively ($p < 0.05$).

Atmospheric pCO_{2a} can be related to global mean C:P assuming constant phosphate inventory, total buffered carbon in the ocean ($C_{buffered}$), and pCO_2 when OCS_{soft} is zero ($c_1 = 651$ ppm):

$$pCO_{2a} \cong c_1 \cdot e^{-\frac{OCS_{soft}}{C_{buffered}}} = c_1 \cdot e^{-\frac{r_{C:P} \cdot (\overline{PO_4} - \overline{PO_{4pref}}) \cdot V_{oc}}{C_{buffered}}} \quad (4)$$

The definition of "buffered carbon" ($C_{buffered}$) follows that of previous studies (Goodwin et al., 2007; Marinov, Follows, et al., 2008; Marinov, Gnanadesikan, et al., 2008):

$$C_{buffered} = M_a \cdot pCO_{2a} + V_{oc} \cdot \overline{DIC_{eq}}/R \cong \text{constant}$$

where M_a is the mass of the atmosphere, R is the Revelle buffer factor, and $\overline{DIC_{eq}}$ is the globally averaged surface equilibrium DIC.

We posit that the global mean C:P of remineralization ($r_{C:P}$) can be predicted as the ratio between globally integrated flux of POC and POP in the twilight zone:

$$r_{C:P} \cong \frac{\int_{z_o}^{z'} F_{C,0} \left(\frac{z}{z_o}\right)^{-b_C} dz}{\int_{z_o}^{z'} F_{P,0} \left(\frac{z}{z_o}\right)^{-b_P} dz} = r_{C:P}(z_0) \cdot \frac{\int_{z_o}^{z'} \left(\frac{z}{z_o}\right)^{-b_C} dz}{\int_{z_o}^{z'} \left(\frac{z}{z_o}\right)^{-b_P} dz} \quad (5)$$

where $r_{C:P}(z_0)$ is the global mean C:P of NPP in the euphotic zone at depth z_0; b_P and b_C are Martin's b exponent for POP and POC, respectively, and z' is the bottom of the depth of the twilight zone. For theoretical prediction of the global mean $r_{C:P}$ from Equation (5), we use fixed surface reference depth z_0 of 100 m and tested different mesopelagic depth horizons z' (250, 1000, and 2000 m). We compared true OCS_{soft} and $pCO2_a$ from the model output with the theoretical predictions based on Equations (3) – (5) and assessed how well $r_{C:P}$ could be estimated from the Martin b parameters alone.

Figure 3 illustrates the relationship between $r_{C:P}$ and the strength of the soft-tissue pump at steady-state. Each steady state model results with different values of b_C are shown as individual points with different colors. Theoretical predictions with different mesopelagic depth horizons z' are shown with lines, and the depth selection z' of 1000 m best matches the model results. A good agreement between the model result and theory gives us

confidence that remineralization occurring in the top 1000 m is a vital determinant of the $r_{C:P,}$ and much of the change in $r_{C:P}$ can be explained by preferential remineralization of POP over POC occurring in the twilight zone (between 250 - 1000 m) and not in the epipelagic or bathypelagic regions of the ocean. If z' is less than approximately 1000 m, the strength of the soft-tissue pump is underestimated for a given value of $r_{C:P,}$ while selecting z' that is too deep leads to an overestimation of the soft-tissue pump.

Our model results suggest that $r_{C:P}$ can change the strength of ocean soft-tissue pump and atmospheric CO_2 drawdown in two ways. First is via a change in the surface C:P ratio of productivity, $r_{C:P}(z_0)$, and this effect can be visualized by comparing the model output with fixed C:P ("Redfield") and the "Control ($b_c = b_p$)" run with variable C:P at the surface but no preferential remineralization at depth. Incorporating variable surface C:P can increase carbon export at 100 m by 3.0 PgC yr^{-1} compared to the Redfield run and increase the total carbon storage by 422 PgC or 21% (Table S5). It is important to note that this mechanism implicitly assumes that small cells are exported more efficiently if the increase in C:P of phytoplankton is tied to the reduction in the weighted size of the phytoplankton.

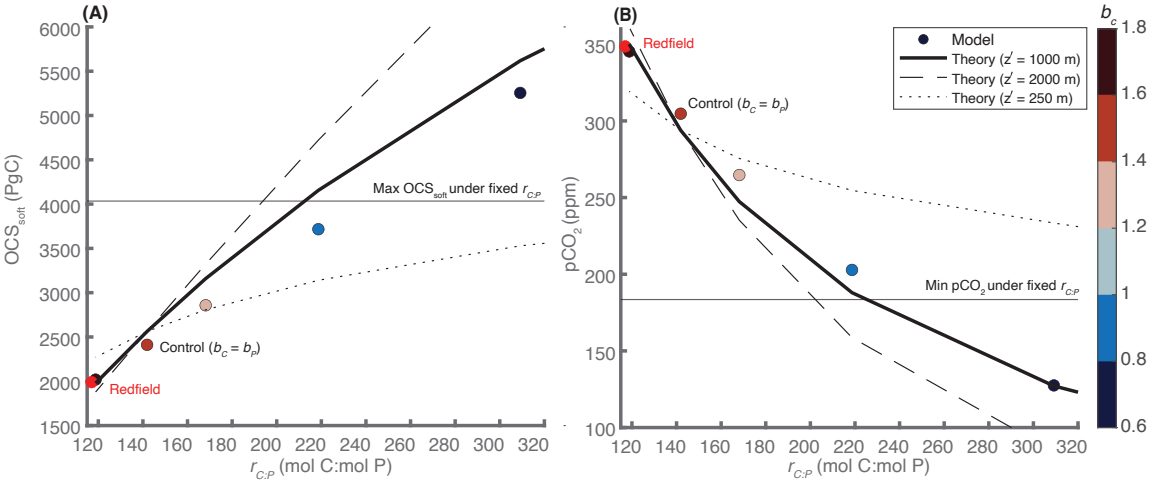

Figure 3. Comparing model and theoretical prediction on the influence of $r_{C:P}$ on ocean carbon storage at steady state. The relationship between $r_{C:P}$ and (a) ocean carbon storage due to soft-tissue pump and (b) atmospheric CO_2. In both panels, model results are shown with dots and theoretical predictions with different twilight zone depth range z' is shown with black lines. The color for plots indicates different Martin *b* parameter for POC used in the simulations. Also shown are threshold OCS_{soft} and pCO_2 when the entire phosphate is in the regenerated form under fixed $r_{C:P}$ of 117.

The second effect for strengthening soft-tissue pump is via an increase in remineralization depth profile of POC from reducing b_C. The global mean C:P remineralization ratio, $r_{C:P,}$ increases from 142 in the control run with no preferential remineralization to as high as 309 when b_c is roughly halved from 1.46 to 0.75. Halving b_c in the model decreases pCO_2 by ~180 ppm from 305 ppm to 128 ppm and more than doubles the carbon storage by the soft-tissue pump. Given that the expected $pCO_{2,}$ when the entire PO_4 reservoir is in the regenerated form at a fixed $r_{C:P}$ of 117, is ~183 ppm, this level of reduction in pCO_2 is extremely large and perhaps unlikely to occur. However, given the large spread in b_c required to explain the observed C:P of POM flux (Figure 1), our sensitivity model runs indicate the potential of particle flux stoichiometry to significantly perturb the global carbon cycle.

An increase in the particle $r_{C:P}$ in the twilight zone and the subsequent strengthening of soft-tissue carbon pump leads to reduction of DIC in the surface and more DIC sequestration in the mid to deep ocean (Figure S3). In the "Control" model run with variable C:P at the surface but with no change in C:P at depth, ΔDIC from the Redfield run is mainly limited in the top 1000 m, and the carbon sequestration signal does not penetrate to the deep ocean (Figure S3c, d). However, when we allow the depth-dependent increase in POC:POP flux via assigning the lower value of b_C, the signal of variable stoichiometry can potentially readily reach the deep ocean. The largest DIC increase occurs in the deep North Pacific Ocean, reflecting the greater accumulation of respired carbon along the deep branch of the overturning circulation (Figure S3e, f). Accumulation of DIC in the deep Pacific is accompanied by a considerable reduction of DIC concentration in the surface ocean and NADW, which is indicative of the subduction of the DIC deplete surface water transported poleward. Our result is unique in that redistribution of DIC can occur without a change in the nutrient distribution, and the change in DIC distribution is entirely through the change in particle export stoichiometry.

4. Discussion and Outlook

We do not currently have a good understanding of the mechanisms that can lead to an increase in C:P of sinking POM fluxes in the twilight zone. However, previous studies (Broecker, 1982b, 1982a; Wakeham et al., 1984) speculated that decoupling of POC and POP remineralization could occur at least three ways: (1) selective removal of the more labile organic matter fractions during the digestive process of zooplankton, (2) formation of fecal pellets enriched with non-labile organic matter such as fiber, and (3) consolidation of fragmented sloppy feeding material and fecal material into larger sinking particles.

Since a large proportion of phytoplankton biomass produced in the surface ocean is eaten by zooplankton (Menzel, 1974), C:N:P of sinking POM could also vary with the quantity and quality of phytoplankton that have been consumed by zooplankton (Knauer et al., 1979; Polimene et al., 2017). For example, when food quality is low (i.e., high C:P of prey), zooplankton retains nutritive elements such as P and N while releasing crude fiber carbon behind as feces leading to high C:P of fecal pellets (Steinberg & Landry, 2017). In contrast, when the food quality is high, fecal matter C:N:P would be close to phytoplankton C:N:P as the large amount of P and N remain in the feces (Sterner, 1990; Tamelander et al., 2012). Therefore predator-prey interactions and prey stoichiometric composition are likely to be essential drivers of variability in C:P of sinking particles (Bach et al., 2020) and provide plausible reasoning why there is a larger positive deviation of C:P of sinking POM from surface suspended POM in the oligotrophic regions (e.g., Subtropical North Pacific) but smaller positive deviation in more nutrient-rich regions (e.g., Subpolar North Pacific).

Microbial transformation of sinking particles can further give rise to C:P with depth if microbes attached to the particles preferentially remineralize P over C (Karl et al., 1996; Taylor et al., 1986). For dissolved organic matter (DOM), the preferential remineralization of P over C via microbes have been extensively documented (Clark et al., 1998; Duhamel et al., 2021; Loh & Bauer, 2000; Lønborg et al., 2009). However, preferential remineralization of POM is somewhat more uncertain because the biochemical compositions of DOM and POM are quite different (Loh & Bauer, 2000). Using 31P-NMR spectroscopy, it has been shown that organic P compounds in sinking POM are generally similar to that of live phytoplankton and significantly different than in the DOM pool (Paytan et al., 2003). Furthermore, the large sinking particles are generally poor habitats for bacterial growth (Cho & Azam, 1988; Karl et al., 1988). Although preferential removal of different types of particulate organic phosphorus compounds, such as phosphonates relative to phosphoesters, have been observed (Benitez-Nelson et al., 2004), and bacteria are known to have a greater tendency for consuming P than C from their food substrates in both open ocean and coastal waters (Gundersen et al., 2002), we do not currently have a good understanding of mechanisms how bacteria attached to sinking POM can preferentially remineralize P over C (Benitez-Nelson, 2000; Benitez-Nelson et al., 2004).

Physical mechanisms such as abiotic particle fragmentation that physically removes P may also increase the C:P flux ratio at depth. It has been suggested that the smaller, older refractory particles that have undergone more fragmentation contribute a greater fraction of POM collected in the deeper trap samples because smaller particles generally have a longer residence time in the oceans (Karl et al., 1988; Wakeham et al., 1984). Physical mixing

and circulation are also likely to be vital in explaining why C:P flux ratios do not continue to increase indefinitely. For example, the C:P flux ratio at HOT at 4000 m is ~ 200:1 (Karl et al., 2012) and is not noticeably higher than the C:P of suspended POM in the surface. As nutrient concentrations in the deep ocean show that the globally averaged bulk of organic matter remineralization occurs in approximately Redfield ratio (Anderson & Sarmiento, 1994), the physical mechanisms maybe playing critical roles in averaging the signal of elevated POC:POP in the surface and twilight zone from reaching the deep ocean (Shaffer et al., 1999; Weber & Deutsch, 2010). A further investigation is required for deciphering different physical and biogeochemical mechanisms responsible for modulating C:P flux stoichiometry in the different depth horizons.

Ocean biogeochemical models are beginning to incorporate flexible C:N:P of phytoplankton and are investigating their roles in the global carbon cycle both in the modern and the palaeoceanographic context (Kwiatkowski et al., 2018; Matsumoto et al., 2020; Moreno et al., 2018; Ödalen et al., 2020; Séférian et al., 2020). However, most models do not yet explicitly consider a change in the elemental stoichiometry of POM once it leaves below the euphotic zone. Here, we have shown the feasibility of a simple approach in changing the C:P of sinking POM by assigning different Martin parameter *b* values for POC and POP (Figure 2). Observations show that different Martin *b* values should be assigned for different elements and molecules, including iron, silica, and chlorophyll (Boyd et al., 2017; Buesseler et al., 2007). In future studies, models could explore how the spatially variable values of element-specific Martin *b* could impact the export strength of the carbon pump. In this regard, other mathematical forms of remineralization profiles such as exponential function (Armstrong et al., 2001; Lauderdale & Cael, 2021; Pavia et al., 2019) may be more realistic than the Martin power-law as it can prevent the flux stoichiometry from increasing indefinitely with depth. In addition to modeling passive fluxes, models also need to consider active transport of material via vertically migrating animals and how they change C:N:P flux stoichiometry in the twilight zone (Hannides et al., 2009; Saba et al., 2021; Schiettekatte et al., 2020).

In summary, we showed through the combination of observation, theory, and numerical modeling that the change in the elemental stoichiometry of sinking POM in the twilight zone could be playing a significant role in ocean biogeochemistry. Our new data compilation supports the notion that preferential removal of P over C of sinking POM at depth is occurring globally. This has an important implication for the global carbon cycle, and we showed using a 3D model and theory that C:P variability in the subsurface can significantly modulate the strength of carbon sequestration by at least 20%. However, many biogeochemical processes in the ocean twilight zone that govern particle transfer are still enigmatic (Boyd et al., 2019; Robinson et al., 2010). Future studies using new

technologies such as Underwater Vision Profilers, robots (Yoerger et al., 2021), and autonomous Argo floats (Briggs et al., 2020) could significantly advance our current understanding of particle dynamics in the twilight zone (A. Martin et al., 2020).

Acknowledgments

This study was supported by the U.S. National Science Foundation (OCE-1827948). In addition, TT acknowledges support from the Simons Foundation Postdoctoral Fellowships in Marine Microbial Ecology. We thank Samar Khatiwala for providing technical support on TMM and Iris Kriest for scripts to analyze the model output. Numerical modeling and analysis were carried out using resources at the University of Minnesota Supercomputing Institute. Ocean biogeochemical model codes are available in the author's GitHub (https://github.com/tanio003/tmm/tree/TT_Release) and are archived in Zenodo (http://doi.org/10.5281/zenodo.4960404). Model input and output files are pending approval for public archive in Dryad (https://doi.org/10.5061/dryad.70rxwdbx). The temporary access link to the model data files for the peer-review process is as following:

https://datadryad.org/stash/share/7JvpjGY70Dr4AVgZsPR6962LIDREeLhHcSp9BU69IYA

References

Anderson, L. A., & Sarmiento, J. L. (1994). Redfield ratios of remineralization determined by nutrient data analysis. *Global Biogeochemical Cycles*, *8*(1), 65–80. https://doi.org/10.1029/93GB03318

Antia, A. N. (2005). Solubilization of particles in sediment traps: revising the stoichiometry of mixed layer export. *Biogeosciences*, *2*(2), 189–204. https://doi.org/10.5194/bg-2-189-2005

Armstrong, R. A., Lee, C., Hedges, J. I., Honjo, S., & Wakeham, S. G. (2001). A new, mechanistic model for organic carbon fluxes in the ocean based on the quantitative association of POC with ballast minerals. *Deep-Sea Research Part II: Topical Studies in Oceanography*, *49*(1–3), 219–236. https://doi.org/10.1016/S0967-0645(01)00101-1

Bach, L. T., Paul, A. J., Boxhammer, T., von der Esch, E., Graco, M., Schulz, K. G., et al. (2020). Factors controlling plankton community production, export flux, and particulate matter stoichiometry in the coastal upwelling system off Peru. *Biogeosciences*, *17*(19), 4831–4852. https://doi.org/10.5194/bg-17-4831-2020

Benitez-Nelson, C. R. (2000). The biogeochemical cycling of phosphorus in marine systems. *Earth-Science Reviews*, *51*(1–4), 109–135. https://doi.org/10.1016/S0012-8252(00)00018-0

Benitez-Nelson, C. R., O'Neill, L., Kolowith, L. C., Pellechia, P., & Thunell, R. (2004). Phosphonates and particulate organic phosphorus cycling in an anoxic marine basin. *Limnology and Oceanography*, *49*(5), 1593–1604. https://doi.org/10.4319/lo.2004.49.5.1593

Benitez-Nelson, C. R., O'Neill Madden, L. P., Styles, R. M., Thunell, R. C., & Astor, Y. (2007). Inorganic and organic sinking particulate phosphorus fluxes across the oxic/anoxic water column of Cariaco Basin, Venezuela. *Marine Chemistry*, *105*(1–2), 90–100. https://doi.org/10.1016/j.marchem.2007.01.007

Boersma, M., Becker, C., Malzahn, A. M., & Vernooij, S. (2009). Food chain effects of nutrient limitation in

primary producers. *Marine and Freshwater Research*, *60*(10), 983–989. https://doi.org/10.1071/MF08240
Boyd, P. W., Ellwood, M. J., Tagliabue, A., & Twining, B. S. (2017, March 1). Biotic and abiotic retention, recycling and remineralization of metals in the ocean. *Nature Geoscience*. Nature Publishing Group. https://doi.org/10.1038/ngeo2876
Boyd, P. W., Claustre, H., Levy, M., Siegel, D. A., & Weber, T. S. (2019). Multi-faceted particle pumps drive carbon sequestration in the ocean. *Nature*, *568*(7752), 327–335. https://doi.org/10.1038/s41586-019-1098-2
Briggs, N., Dall'Olmo, G., & Claustre, H. (2020). Major role of particle fragmentation in regulating biological sequestration of CO2 by the oceans. *Science*, *367*(6479), 791–793. https://doi.org/10.1126/science.aay1790
Broecker, W. S. (1982a). Glacial to interglacial changes in ocean chemistry. *Progress in Oceanography*, *11*(2), 151–197. https://doi.org/10.1016/0079-6611(82)90007-6
Broecker, W. S. (1982b). Ocean chemistry during glacial time. *Geochimica et Cosmochimica Acta*, *46*(10), 1689–1705. https://doi.org/10.1016/0016-7037(82)90110-7
Buesseler, K. O., Lamborg, C. H., Boyd, P. W., Lam, P. J., Trull, T. W., Bidigare, R. R., et al. (2007). Revisiting carbon flux through the ocean's twilight zone. *Science*, *316*(5824), 567–570. https://doi.org/10.1126/science.1137959
Cho, B. C., & Azam, F. (1988). Major role of bacteria in biogeochemical fluxes in the ocean's interior. *Nature*, *332*(6163), 441–443.
Christian, J. R., Lewis, M. R., & Karl, D. M. (1997). Vertical fluxes of carbon, nitrogen, and phosphorus in the North Pacific Subtropical Gyre near Hawaii. *Journal of Geophysical Research: Oceans*, *102*(C7), 15667–15677. https://doi.org/10.1029/97JC00369
Clark, L. L., Ingall, E. D., & Benner, R. (1998). Marine phosphorus is selectively remineralized. *Nature*, *393*(6684), 426–426. https://doi.org/10.1038/30881
Duhamel, S., Diaz, J. M., Adams, J. C., Djaoudi, K., Steck, V., & Waggoner, E. M. (2021). Phosphorus as an integral component of global marine biogeochemistry. *Nature Geoscience*, *14*(6), 359–368. https://doi.org/10.1038/s41561-021-00755-8
Duteil, O., Koeve, W., Oschlies, A., Aumont, O., Bianchi, D., Bopp, L., et al. (2012). Preformed and regenerated phosphate in ocean general circulation models: can right total concentrations be wrong? *Biogeosciences*, *9*(5), 1797–1807. https://doi.org/10.5194/bg-9-1797-2012
Engel, A., Wagner, H., Le Moigne, F. A. C., & Wilson, S. T. (2017). Particle export fluxes to the oxygen minimum zone of the eastern tropical North Atlantic. *Biogeosciences*, *14*(7), 1825–1838. https://doi.org/10.5194/bg-14-1825-2017
Faul, K. L., Paytan, A., & Delaney, M. L. (2005). Phosphorus distribution in sinking oceanic particulate matter. *Marine Chemistry*, *97*(3–4), 307–333. https://doi.org/10.1016/j.marchem.2005.04.002
Galbraith, E. D., & Martiny, A. C. (2015). A simple nutrient-dependence mechanism for predicting the stoichiometry of marine ecosystems. *Proceedings of the National Academy of Sciences*, *112*(27), 8199–8204. https://doi.org/10.1073/pnas.1423917112
Garcia, H., Weathers, K. W., Paver, C. R., Smolyar, I., Boyer, T. P., Locarnini, R. A., et al. (2018). World Ocean Atlas 2018. Volume 4: Dissolved Inorganic Nutrients (phosphate, nitrate and nitrate+nitrite, silicate). In A. Mishonov (Ed.), *NOAA Atlas NESDIS 84* (Vol. 84, p. 35).
Giering, S. L. C., Sanders, R., Lampitt, R. S., Anderson, T. R., Tamburini, C., Boutrif, M., et al. (2014). Reconciliation of the carbon budget in the ocean's twilight zone. *Nature*, *507*(7493), 480–483. https://doi.org/10.1038/nature13123
Goodwin, P., Williams, R. G., Follows, M. J., & Dutkiewicz, S. (2007). Ocean-atmosphere partitioning of anthropogenic carbon dioxide on centennial timescales. *Global Biogeochemical Cycles*, *21*(1), 1–10. https://doi.org/10.1029/2006GB002810

Grabowski, E., Letelier, R. M., Laws, E. A., & Karl, D. M. (2019). Coupling carbon and energy fluxes in the North Pacific Subtropical Gyre. *Nature Communications*, *10*(1), 1895. https://doi.org/10.1038/s41467-019-09772-z

Gundersen, K., Heldal, M., Norland, S., Purdie, D. A., & Knap, A. H. (2002). Elemental C, N, and P cell content of individual bacteria collected at the Bermuda Atlantic Time-series Study (BATS) site. *Limnology and Oceanography*, *47*(5), 1525–1530. https://doi.org/10.4319/lo.2002.47.5.1525

Hannides, C. C. S., Landry, M. R., Benitez-Nelson, C. R., Styles, R. M., Montoya, J. P., & Karl, D. M. (2009). Export stoichiometry and migrant-mediated flux of phosphorus in the North Pacific Subtropical Gyre. *Deep-Sea Research Part I: Oceanographic Research Papers*, *56*(1), 73–88. https://doi.org/10.1016/j.dsr.2008.08.003

Ito, T., & Follows, M. J. (2005). Preformed phosphate, soft tissue pump and atmospheric CO2. *Journal of Marine Research*, *63*(4), 813–839. https://doi.org/10.1357/0022240054663231

Karl, D. M., Knauer, G. A., & Martin, J. H. (1988). Downward flux of particulate organic matter in the ocean: a particle decomposition paradox. *Nature*, *332*(6163), 438–441. https://doi.org/10.1038/332438a0

Karl, D. M., Christian, J. R., Dore, J. E., Hebel, D. V., Letelier, R. M., Tupas, L. M., & Winn, C. D. (1996). Seasonal and interannual variability in primary production and particle flux at Station ALOHA. *Deep Sea Research Part II: Topical Studies in Oceanography*, *43*(2–3), 539–568. https://doi.org/10.1016/0967-0645(96)00002-1

Karl, D. M., Church, M. J., Dore, J. E., Letelier, R. M., & Mahaffey, C. (2012). Predictable and efficient carbon sequestration in the North Pacific Ocean supported by symbiotic nitrogen fixation. *Proceedings of the National Academy of Sciences of the United States of America*, *109*(6), 1842–1849. https://doi.org/10.1073/pnas.1120312109

Khatiwala, S. (2007). A computational framework for simulation of biogeochemical tracers in the ocean. *Global Biogeochemical Cycles*, *21*(3). https://doi.org/10.1029/2007GB002923

Khatiwala, S., Visbeck, M., & Cane, M. A. (2005). Accelerated simulation of passive tracers in ocean circulation models. *Ocean Modelling*, *9*(1), 51–69. https://doi.org/10.1016/j.ocemod.2004.04.002

Khatiwala, S., Primeau, F. W., & Holzer, M. (2012). Ventilation of the deep ocean constrained with tracer observations and implications for radiocarbon estimates of ideal mean age. *Earth and Planetary Science Letters*, *325–326*, 116–125. https://doi.org/10.1016/j.epsl.2012.01.038

Knauer, G. A., Martin, J. H., & Bruland, K. W. (1979). Fluxes of particulate carbon, nitrogen, and phosphorus in the upper water column of the northeast Pacific. *Deep Sea Research Part A. Oceanographic Research Papers*, *26*(1), 97–108. https://doi.org/10.1016/0198-0149(79)90089-X

Kriest, I., & Oschlies, A. (2013). Swept under the carpet: Organic matter burial decreases global ocean biogeochemical model sensitivity to remineralization length scale. *Biogeosciences*, *10*(12), 8401–8422. https://doi.org/10.5194/bg-10-8401-2013

Kriest, I., & Oschlies, A. (2015). MOPS-1.0: Towards a model for the regulation of the global oceanic nitrogen budget by marine biogeochemical processes. *Geoscientific Model Development*, *8*(9), 2929–2957. https://doi.org/10.5194/gmd-8-2929-2015

Kriest, I., Kähler, P., Koeve, W., Kvale, K. F., Sauerland, V., & Oschlies, A. (2020). One size fits all? Calibrating an ocean biogeochemistry model for different circulations. *Biogeosciences*, *17*(12), 3057–3082. https://doi.org/10.5194/bg-17-3057-2020

Kwiatkowski, L., Aumont, O., Bopp, L., & Ciais, P. (2018). The Impact of Variable Phytoplankton Stoichiometry on Projections of Primary Production, Food Quality, and Carbon Uptake in the Global Ocean. *Global Biogeochemical Cycles*, *32*(4), 516–528. https://doi.org/10.1002/2017GB005799

Kwon, E. Y., Primeau, F. W., & Sarmiento, J. L. (2009). The impact of remineralization depth on the air-sea carbon balance. *Nature Geoscience*, *2*(9), 630–635. https://doi.org/10.1038/ngeo612

512 Lamborg, C. H., Buesseler, K. O., Valdes, J., Bertrand, C. H., Bidigare, R., Manganini, S., et al. (2008). The flux
513 of bio- and lithogenic material associated with sinking particles in the mesopelagic “twilight zone” of the
514 northwest and North Central Pacific Ocean. *Deep Sea Research Part II: Topical Studies in Oceanography*,
515 *55*(14–15), 1540–1563. https://doi.org/10.1016/j.dsr2.2008.04.011
516 Lauderdale, J. M., & Cael, B. B. (2021). Impact of Remineralization Profile Shape on the Air-Sea Carbon Balance.
517 *Geophysical Research Letters*, *48*(7), e2020GL091746. https://doi.org/10.1029/2020GL091746
518 Loh, A. N., & Bauer, J. E. (2000). Distribution, partitioning and fluxes of dissolved and particulate organic C, N
519 and P in the eastern North Pacific and Southern Oceans. *Deep Sea Research Part I: Oceanographic*
520 *Research Papers*, *47*(12), 2287–2316. https://doi.org/10.1016/S0967-0637(00)00027-3
521 Lomas, M. W., Burke, A. L., Lomas, D. A., Bell, D. W., Shen, C., Dyhrman, S. T., & Ammerman, J. W. (2010).
522 Sargasso Sea phosphorus biogeochemistry: An important role for dissolved organic phosphorus (DOP).
523 *Biogeosciences*, *7*(2), 695–710. https://doi.org/10.5194/bg-7-695-2010
524 Lønborg, C., Davidson, K., Álvarez-Salgado, X. A., & Miller, A. E. J. (2009). Bioavailability and bacterial
525 degradation rates of dissolved organic matter in a temperate coastal area during an annual cycle. *Marine*
526 *Chemistry*, *113*(3–4), 219–226. https://doi.org/10.1016/j.marchem.2009.02.003
527 Marinov, I., Follows, M. J., Gnanadesikan, A., Sarmiento, J. L., & Slater, R. D. (2008). How does ocean biology
528 affect atmospheric p CO 2 ? Theory and models. *Journal of Geophysical Research*, *113*(C7), C07032.
529 https://doi.org/10.1029/2007JC004598
530 Marinov, I., Gnanadesikan, A., Sarmiento, J. L., Toggweiler, J. R., Follows, M., & Mignone, B. K. (2008). Impact
531 of oceanic circulation on biological carbon storage in the ocean and atmospheric p CO 2. *Global*
532 *Biogeochemical Cycles*, *22*(3), n/a-n/a. https://doi.org/10.1029/2007GB002958
533 Martin, A., Boyd, P., Buesseler, K., Cetinic, I., Claustre, H., Giering, S., et al. (2020). The oceans’ twilight zone
534 must be studied now, before it is too late. *Nature*, *580*(7801), 26–28. https://doi.org/10.1038/d41586-020-
535 00915-7
536 Martin, J. H., Knauer, G. A., Karl, D. M., & Broenkow, W. W. (1987). VERTEX: carbon cycling in the northeast
537 Pacific. *Deep Sea Research Part A. Oceanographic Research Papers*, *34*(2), 267–285.
538 https://doi.org/10.1016/0198-0149(87)90086-0
539 Martiny, A. C., Pham, C. T. A., Primeau, F. W., Vrugt, J. A., Moore, J. K., Levin, S. A., & Lomas, M. W. (2013).
540 Strong latitudinal patterns in the elemental ratios of marine plankton and organic matter. *Nature Geoscience*,
541 *6*(4), 279–283. https://doi.org/10.1038/ngeo1757
542 Martiny, A. C., Vrugt, J. A., & Lomas, M. W. (2014). Concentrations and ratios of particulate organic carbon,
543 nitrogen, and phosphorus in the global ocean. *Scientific Data*, *1*, 140048.
544 https://doi.org/10.1038/sdata.2014.48
545 Matsumoto, K. (2007). Biology-mediated temperature control on atmospheric pCO2 and ocean biogeochemistry.
546 *Geophysical Research Letters*, *34*(20), 1–5. https://doi.org/10.1029/2007GL031301
547 Matsumoto, K., Rickaby, R., & Tanioka, T. (2020). Carbon Export Buffering and CO2 Drawdown by Flexible
548 Phytoplankton C:N:P Under Glacial Conditions. *Paleoceanography and Paleoclimatology*, *35*(7).
549 https://doi.org/10.1029/2019PA003823
550 Menzel, D. W. (1974). Primary productivity, dissolved and particulate organic matter, and the sites of oxidation
551 of organic matter. *The Sea. Marine Chemistry.*, *5*, 654–678.
552 Menzel, D. W., & Ryther, J. H. (1964). The Composition of Particulate Organic Matter in the Western North
553 Atlantic. *Limnology and Oceanography*, *9*(2), 179–186. https://doi.org/10.4319/lo.1964.9.2.0179
554 Minster, J. F., & Boulahdid, M. (1987). Redfield ratios along isopycnal surfaces-a complementary study. *Deep*
555 *Sea Research Part A, Oceanographic Research Papers*, *34*(12), 1981–2003. https://doi.org/10.1016/0198-
556 0149(87)90094-X
557 Moreno, A. R., Hagstrom, G. I., Primeau, F. W., Levin, S. A., & Martiny, A. C. (2018). Marine phytoplankton

stoichiometry mediates nonlinear interactions between nutrient supply, temperature, and atmospheric CO2. *Biogeosciences*, *15*(9), 2761–2779. https://doi.org/10.5194/bg-15-2761-2018

Ödalen, M., Nycander, J., Ridgwell, A., Oliver, K. I. C., Peterson, C. D., & Nilsson, J. (2020). Variable C/P composition of organic production and its effect on ocean carbon storage in glacial-like model simulations. *Biogeosciences*, *17*(8), 2219–2244. https://doi.org/10.5194/bg-17-2219-2020

Pavia, F. J., Anderson, R. F., Lam, P. J., Cael, B. B., Vivancos, S. M., Fleisher, M. Q., et al. (2019). Shallow particulate organic carbon regeneration in the South Pacific Ocean. *Proceedings of the National Academy of Sciences of the United States of America*, *116*(20), 9753–9758. https://doi.org/10.1073/pnas.1901863116

Paytan, A., Cade-Menun, B. J., McLaughlin, K., & Faul, K. L. (2003). Selective phosphorus regeneration of sinking marine particles: evidence from 31P-NMR. *Marine Chemistry*, *82*(1–2), 55–70. https://doi.org/10.1016/S0304-4203(03)00052-5

Polimene, L., Sailley, S. F., Clark, D., Mitra, A., & Allen, J. I. (2017). Biological or microbial carbon pump? The role of phytoplankton stoichiometry in ocean carbon sequestration. *Journal of Plankton Research*, *39*(2), 180–186. https://doi.org/10.1093/plankt/fbw091

R Core Team. (2021). R: A Language and Environment for Statistical Computing. Vienna, Austria. Retrieved from https://www.r-project.org/

Robinson, C., Steinberg, D. K., Anderson, T. R., Arístegui, J., Carlson, C. A., Frost, J. R., et al. (2010). Mesopelagic zone ecology and biogeochemistry – a synthesis. *Deep Sea Research Part II: Topical Studies in Oceanography*, *57*(16), 1504–1518. https://doi.org/10.1016/j.dsr2.2010.02.018

Saba, G. K., Burd, A. B., Dunne, J. P., Hernández-León, S., Martin, A. H., Rose, K. A., et al. (2021). Toward a better understanding of fish-based contribution to ocean carbon flux. *Limnology and Oceanography*, *66*(5), 1639–1664. https://doi.org/10.1002/lno.11709

Sarmiento, J. L., & Toggweiler, J. R. (1984). A new model for the role of the oceans in determining atmospheric PCO2. *Nature*, *308*(5960), 621–624. https://doi.org/10.1038/308621a0

Schiettekatte, N. M. D., Barneche, D. R., Villéger, S., Allgeier, J. E., Burkepile, D. E., Brandl, S. J., et al. (2020). Nutrient limitation, bioenergetics and stoichiometry: A new model to predict elemental fluxes mediated by fishes. *Functional Ecology*, *34*(9), 1857–1869. https://doi.org/10.1111/1365-2435.13618

Séférian, R., Berthet, S., Yool, A., Palmiéri, J., Bopp, L., Tagliabue, A., et al. (2020). Tracking Improvement in Simulated Marine Biogeochemistry Between CMIP5 and CMIP6. *Current Climate Change Reports*, *6*(3), 95–119. https://doi.org/10.1007/s40641-020-00160-0

Shaffer, G., Bendtsen, J., & Ulloa, O. (1999). Fractionation during remineralization of organic matter in the ocean. *Deep-Sea Research Part I: Oceanographic Research Papers*, *46*(2), 185–204. https://doi.org/10.1016/S0967-0637(98)00061-2

Sigman, D. M., & Boyle, E. A. (2000). Glacial/interglacial variations in atmospheric carbon dioxide. *Nature*, *407*(6806), 859–869. https://doi.org/10.1038/35038000

Stammer, D., Ueyoshi, K., Köhl, A., Large, W. G., Josey, S. A., & Wunsch, C. (2004). Estimating air-sea fluxes of heat, freshwater, and momentum through global ocean data assimilation. *Journal of Geophysical Research C: Oceans*, *109*(5), C05023. https://doi.org/10.1029/2003JC002082

Steinberg, D. K., & Landry, M. R. (2017). Zooplankton and the Ocean Carbon Cycle. *Annual Review of Marine Science*, (October 2016), 1–32. https://doi.org/10.1146/annurev-marine-010814-015924

Sterner, R. W. (1990). The Ratio of Nitrogen to Phosphorus Resupplied by Herbivores: Zooplankton and the Algal Competitive Arena. *The American Naturalist*, *136*(2), 209. https://doi.org/10.1086/285092

Tamelander, T., Aubert, A. B., & Riser, C. W. (2012). Export stoichiometry and contribution of copepod faecal pellets to vertical flux of particulate organic carbon, nitrogen and phosphorus. *Marine Ecology Progress Series*, *459*, 17–28. https://doi.org/10.3354/meps09733

Tanioka, T., & Matsumoto, K. (2017). Buffering of Ocean Export Production by Flexible Elemental Stoichiometry

of Particulate Organic Matter. *Global Biogeochemical Cycles*, *31*(10), 1528–1542. https://doi.org/10.1002/2017GB005670

Tanioka, T., & Matsumoto, K. (2020). A meta-analysis on environmental drivers of marine phytoplankton C : N : P. *Biogeosciences*, *17*(11), 2939–2954. https://doi.org/10.5194/bg-17-2939-2020

Taylor, G., Karl, D. M., & Pace, M. (1986). Impact of bacteria and zooflagellates on the composition of sinking particles: an in situ experiment. *Marine Ecology Progress Series*, *29*, 141–155. https://doi.org/10.3354/meps029141

Teng, Y.-C., Primeau, F. W., Moore, J. K., Lomas, M. W., & Martiny, A. C. (2014). Global-scale variations of the ratios of carbon to phosphorus in exported marine organic matter. *Nature Geoscience*, *7*(12), 895–898. https://doi.org/10.1038/ngeo2303

Wakeham, S. G., Lee, C., Farrington, J. W., & Gagosian, R. B. (1984). Biogeochemistry of particulate organic matter in the oceans: results from sediment trap experiments. *Deep Sea Research Part A. Oceanographic Research Papers*, *31*(5), 509–528. https://doi.org/10.1016/0198-0149(84)90099-2

Weber, T. S., & Deutsch, C. (2010). Ocean nutrient ratios governed by plankton biogeography. *Nature*, *467*(7315), 550–554. https://doi.org/10.1038/nature09403

Yoerger, D. R., Govindarajan, A. F., Howland, J. C., Llopiz, J. K., Wiebe, P. H., Curran, M., et al. (2021). A hybrid underwater robot for multidisciplinary investigation of the ocean twilight zone. *Science Robotics*, *6*(55), eabe1901. https://doi.org/10.1126/scirobotics.abe1901